

Stochastic model for the alignment and tumbling of rigid fibres in two-dimensional turbulent shear flow

Lorenzo Campana,¹ Mireille Bossy,¹ and Jérémie Bec^{1,2}

¹*Université Côte d’Azur, Inria, CNRS, Cemef, Sophia-Antipolis, France*

²*MINES Paris, PSL Research University, CNRS, Cemef, Sophia-Antipolis, France*

Non-spherical particles transported by an anisotropic turbulent flow preferentially align with the mean shear and intermittently tumble when the local strain fluctuates. Such an intricate behaviour is here studied for inertialess, rod-shaped particles embedded in a two-dimensional turbulent flow with homogeneous shear. A Lagrangian stochastic model for the rods angular dynamics is introduced and compared to the results of direct numerical simulations. The model consists in superposing a short-correlated random component to the steady large-scale mean shear, and can thereby be integrated analytically. To reproduce the single-time orientation statistics obtained numerically, it is found that one has to properly account for the combined effect of the mean shear, for anisotropic velocity gradient fluctuations, and for the presence of persistent rotating structures in the flow that bias Lagrangian statistics. The model is then used to address two-time statistics. The notion of tumbling rate is extended to diffusive dynamics by introducing the stationary probability flux of the rods unfolded angle. The model is found to reproduce the long-term effects of an average shear on the mean and the variance of the fibres angular increment. Still, it does not reproduce an intricate behaviour observed in numerics for intermediate times: the unfolded angle is there very similar to a Lévy walk with distributions of increments displaying intermediate power-law tails.

I. INTRODUCTION

The control and prediction of flows seeded with non-spherical particles (fibres, discs, or inclusions with more general shapes) are important in many industrial and natural processes. In papermaking, mechanical properties are regulated by the alignment of cellulose fibres in the pulp [1]. The shape and orientation of fractal soot emitted by combustion engines determines their radiative properties as aerosols [2]. Particles non-spherical shape is key to study the dispersion of pollen and seeds [3], the lifecycle of diatom plankton [4] and sediment transport in rivers [5]. Besides, the addition of fibres in a fluid flow can significantly alter the suspension rheology [6, 7].

In most of these applications, the flow is highly turbulent and the particles rotational dynamics, their alignment and correlations with the flow become of considerable interest. When their size falls in the active turbulent scales, the particles filter the fluid in a complex manner and display a very intricate dynamics. Particles with sizes in the dissipative range have a more tractable behaviour. When their slip velocity is small enough, the local flow has a weak inertia and Stokes solutions can be used to relate the particles translational and rotational dynamics to the local velocity field and its gradient tensor. This approach was introduced by Jeffery [8] and used to investigate various interesting phenomena, such as the tumbling of rods placed in a constant shear flow and subject to thermal fluctuations, and their resulting periodic motions on closed (Jeffery’s) orbits.

In turbulence, fluctuations originate from the small-scale motions of the flow and this affects the angular dynamics of anisotropic particles. Such questions have recently been the subject of a renewed interest. At an experimental level, particle tracking techniques allowed to reconstruct particle orientational dynamics in several turbulent water flows [9–13]. As to numerical studies, they consist in simulating, in addition to the fluid flow, the orientation of particles by integrating Jeffery’s equation along Lagrangian trajectories. Simulations have been carried out in homogeneous isotropic turbulence [14, 15], as well as in turbulent channel flows [16], in two-dimensional convection [17] and in chaotic velocity fields [18]. From a theoretical perspective, most studies consisted in deriving model equations for the probability distribution of orientations, in which turbulent fluctuations are approximated by an effective isotropic diffusion term [19]. We refer the reader to [20] for a recent review of these results. Despite several studies in turbulent channel flows, much needs to be understood in the presence of flow anisotropies.

We here focus on the statistics of alignment and tumbling in the presence of a mean shear, for which we expect spheres and rods to rotate in qualitatively different fashions. When the particle’s Reynolds number is small, the local flow is well approximated by a Stokes flow. If in addition their inertia can be neglected, spheres will rotate with an angular velocity given by half the flow vorticity. Studying the dynamics of ellipsoidal particles in turbulence is a challenging problem because it requires to understand how the Lagrangian statistics of velocity gradients influence the orientation dynamics of particles. A number of recent numerical and theoretical works studied the orientation statistics of non-spherical particles (rods, ellipsoids, disks) by assuming that the velocity field is isotropic and Gaussian, *e.g.* results from the superposition of linear Ornstein–Uhlenbeck processes [14, 21, 22]. This assumption, albeit restrictive, allows for a fully analytical expression of the probability density function of the particles orientation. More refined

models for Lagrangian velocity gradients have been proposed [23–26], with the aim to represent specific features encoded in the tensor, such as the alignment of vorticity with the strain-rate eigenvectors, the rate of deformation and shape of fluid material volumes, non-Gaussian statistics or intermittency. Chevillard and Meneveau [27] have studied the orientation of tri-axial ellipsoids in direct numerical simulations of homogeneous isotropic turbulence and compared their results to Lagrangian stochastic models based on the recent fluid deformation approximation. This approach, which includes realistic strain–vorticity correlations, was moreover used in [28] to develop a stochastic model that accounts for the fluid velocity intermittency. As stressed in [27, 28], coupling these models to the orientation dynamics of non-spherical particles turns out to be a precise and demanding way to assess their accuracy. However, in contrast with the homogeneous and isotropic case, only few analytical results exist on the probability distribution of orientations in flows with a mean shear. The orientation dynamics of rod-like polymers was studied numerically [29] and analytically [30] using the superposition of a mean shear and isotropic fluctuations with short time correlations. The dynamics of semi-flexible objects in an extensional flow was otherwise analysed in [31, 32].

In this article, we rely on the use of direct numerical simulation (DNS) to validate the development of a Lagrangian stochastic model. Our model consists in approximating the flow viewed by the rods as the superposition of a constant shear with a random component corresponding to a chaotic, fluctuating velocity field. In the spirit of classical approaches [33, 34], the fluctuating part is approximated as a Gaussian white-in-time noise with prescribed correlations. The assumption of temporal decorrelation is adequate when the correlation time of the flow is short compared to the time scales of relevance for the rod evolution. Furthermore, such models are a great simplification of real flows and have been successfully applied for analysing transport by turbulent flows [35]. This approach, which is apparently restrictive, has the great advantage to permit analytical derivations. As an instance, we obtain an exact expression for the probability distribution of the rod orientation angle.

The model that we introduce depends on a non-dimensional parameter, the Kubo number $Ku = \tau_I/\tau_\omega$, defined as the ratio between the integral correlation time of the Lagrangian velocity gradient and the timescale obtained from the inverse of its standard deviation. We compare three different models for the effective correlation tensor: The first assumes that the correlations are isotropic without any reference to Ku ; The second introduces anisotropies by directly measuring the instantaneous correlations of the velocity gradient components and requires prescribing the value of Ku ; The third is based on measurements from the DNS of orientation-dependent integral correlation times and provides the model with an effective anisotropic correlation tensor. All three models reproduce qualitatively the preferential alignment of rods with the direction of shear, with an angular distribution that gets more peaked with increasing mean shear. Results show, however, that a good quantitative agreement with DNS is obtained only with the third approach, underlining the importance of accurately reproducing the anisotropies of fluctuations.

Finally, we study the statistics of rod tumbling and of the particles angular velocity. This notion is ill-defined in stochastic models, and we therefore introduce an alternative way to characterise tumbling through the two-time statistics of particles orientation. It relies on estimating the time derivative of the average unfolded angular displacement. The analytic results obtained from our model are compared with DNS measurements, revealing that the model is in quantitative agreement for adequate values of the calibration parameter. However, we point out the limit of Gaussian models that are unable to properly reproduce large fluctuations of the rods angular displacement. Indeed, we observe in DNS that the probability distribution of the orientation increment displays intermediate algebraic tails that are a signature of trapping by the long-living vortical structures of the flow.

Our presentation is organised as follows. In Sec. II we formulate the dynamics of rod-like particles in two-dimensional turbulent flow with homogeneous shear, describe the numerical method used for direct numerical simulation (DNS), and present results on the preferential alignment of rods. Section III then introduces the Lagrangian stochastic model for the rods’ orientation and analytical results for the stationary distribution of the orientation angle. The various choices for the effective gradient correlations are discussed and compared to the results of DNS. Section IV is devoted to two-time statistics and provides a new definition of tumbling rate, which is investigated both numerically in DNS and analytically for the Lagrangian model. Conclusions and open questions are finally drawn in Sec. V.

II. SETTINGS AND DIRECT NUMERICAL SIMULATIONS

A. Two-dimensional turbulence with homogeneous shear

The fluid velocity \mathbf{v} is here assumed to solve the two-dimensional incompressible Navier–Stokes equations

$$\begin{aligned} \partial_t \mathbf{v} + \mathbf{v} \cdot \nabla \mathbf{v} &= -\nabla p + \nu \nabla^2 \mathbf{v} - \alpha (\mathbf{v} - \sigma y \hat{\mathbf{x}}) + \mathbf{f}, \\ \nabla \cdot \mathbf{v} &= 0, \end{aligned} \tag{1}$$

where the fluid has a constant density equal to unity, the pressure p enforces incompressibility, and ν is the kinematic viscosity. The flow experiences a drag with coefficient α to an underlying flow in the x direction that varies linearly

along the y axis with shear rate σ . In the absence of external forcing ($\mathbf{f} = 0$), the fluid velocity relaxes to the two-dimensional shear flow $\mathbf{v}_\infty = \sigma y \hat{\mathbf{x}}$, which is a stable stationary solution to Eq. (1). In order to maintain a developed turbulent state, an input of kinetic energy is provided by the stochastic forcing \mathbf{f} , which is assumed Gaussian with zero mean, homogeneous, isotropic, white in time and concentrated over the large spatial scales. The incompressible turbulent fluctuations $\mathbf{u} = \mathbf{v} - \mathbf{v}_\infty$ are then homogeneous in space and stationary in time. The equations of motion are supplemented with appropriate periodic boundary conditions on a square domain of size L^2 . They read $\mathbf{u}(x + L, y) = \mathbf{u}(x, y)$ and $\mathbf{u}(x, y + L) = \mathbf{u}(x - t \sigma L, y)$.

We perform direct numerical simulations by using a pseudo-spectral solver. To construct periodic solutions that account for the mean flow, we follow [36, 37] and integrate the dynamics of vorticity fluctuation $\omega = \nabla \times \mathbf{u} = \partial_x u_y - \partial_y u_x$ on a distorting frame defined by $x' = x - t \sigma y$, $y' = y$. The integration domain is the two-dimensional torus $[0, 2\pi]^2$ at resolution 128^2 . The distorted grid is regularly shifted back to the Cartesian grid at times multiple of $1/\sigma$. We make use of the vorticity formulation, together with using the Biot–Savard law to obtain the fluctuating velocity \mathbf{u} as a function of the vorticity ω . Time marching uses a second-order Runge–Kutta method, which is explicit for the non-linear term and implicit for the friction and viscous terms. Furthermore, simulations are performed with hyperviscosity and hypofriction in place of the viscous dissipation and linear friction terms appearing in the right-hand side of Eq. (1). The latter two terms are replaced with $(-1)^{p+1} \nu_p \nabla^{2p} \mathbf{v}$ and $(-1)^{q+1} \alpha_q \nabla^{-2q} \mathbf{v}$, respectively. The use of hyperviscosity ($p > 1$) and hypofriction ($q > 0$) is motivated by the resulting reduction of the scale range over which dissipative terms contribute substantially, whereby extending the inertial range for a given spatial resolution [38, 39]. It has been observed that such a modified dissipation might affect velocity statistics at the transition between inertial and dissipative scales [40]. Still, the situations and effects that we consider here are related to the direct cascade of enstrophy, which is only very weakly perturbed.

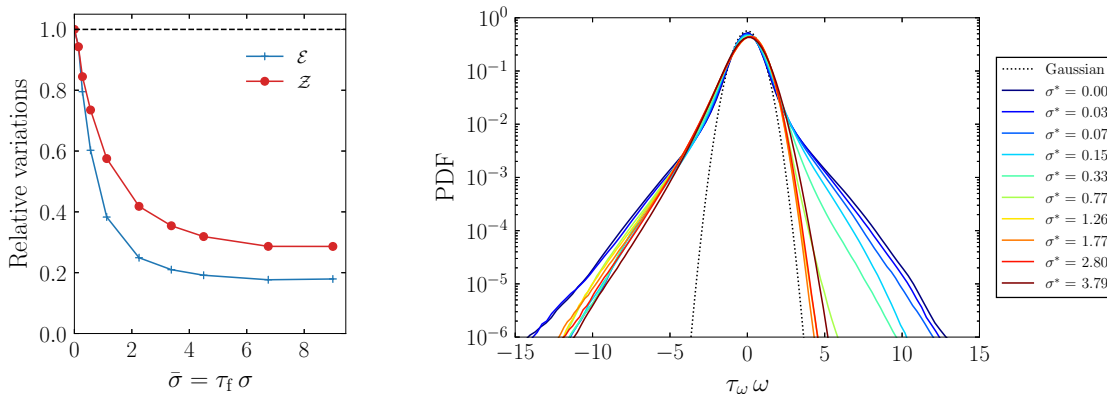


Figure 1: (Colour online) **Left:** Relative evolution of the turbulent kinetic energy $\mathcal{E} = \langle |\mathbf{u}|^2 \rangle / 2$ and enstrophy $\mathcal{Z} = \langle \omega^2 \rangle / 2$ as a function of the dimensionless shear parameter $\bar{\sigma} = \tau_f \sigma$. **Right:** Probability density function (PDF) of the vorticity ω for various values of the shear rate parameter $\sigma^* = \tau_\omega \sigma$.

The power spectrum of the external force is chosen with a Gaussian shape, centred at wavenumber $k_f = 4$ and with variance $\sigma_f = 0.5$. The choice of an additive, white-in-time forcing prescribes the rates ε_I and η_I at which energy and enstrophy are injected in the flow [41]. In particular, we performed several numerical experiments varying the shear rate σ while keeping constant these two injection rates and so, the resulting forcing length scale $\ell_f = (\varepsilon_I / \eta_I)^{1/2}$ and time scale $\tau_f = \eta_I^{-1/3}$. The influence of the mean shear is then naturally weighed by the non-dimensional parameter $\bar{\sigma} = \tau_f \sigma$. As seen in Fig. 1 (left), shear has a strong effect on the energy and enstrophy of turbulent fluctuations: These two global quantities decrease with increasing $\bar{\sigma}$, evidencing a significant reduction of fluctuations. As a consequence, the typical dynamical timescale of the direct cascade $\tau_\omega = \langle \omega^2 \rangle^{-1/2}$ significantly increases with shear. To account for this trend, we introduce another dimensionless shear rate parameter defined as $\sigma^* = \tau_\omega \sigma$.

Besides modifying global budgets, the presence of a mean shear is responsible for the development of anisotropies in the flow. This is evident from the one-point, one-time probability density function (PDF) of the vorticity ω . As can be seen in Fig. 1 (right). Even if the mean value remains zero, shear strongly depletes the distribution of positive (anticyclonic) values, so that vorticity becomes strongly skewed toward negative (cyclonic) values when σ^* increase. At $\sigma^* = 0$, the distribution consists of a Gaussian core, followed by exponential tails, as predicted for instance in [42]. Shear tends to slightly shift the Gaussian core toward positive values. The far exponential tails persist but become skewed. While the negative tail is slightly depleted, the positive one is significantly affected by shear with a decay rate that strongly increases as a function of σ^* . The main effect of shear is thus to bias vortex filaments toward positive vorticities (Gaussian core) and to deplete anticyclonic vortical coherent structures (right tail).

B. Rods dynamics and preferential alignment

The flow is uniformly seeded with tracer particles whose trajectories follow $d\mathbf{X}(t)/dt = \mathbf{v}(\mathbf{X}(t), t)$. Each tracer is assigned with a unit orientation vector \mathbf{p} that evolves according to Jeffery's equation for inertialess rod-like particles [8]

$$\frac{d}{dt}\mathbf{p} = \mathbb{A}\mathbf{p} - (\mathbf{p}^\top \mathbb{A}\mathbf{p})\mathbf{p}, \quad (2)$$

where $\mathbb{A}(t)$ denotes the gradient tensor of the fluid-velocity field \mathbf{v} , evaluated at the particle's position. Its components read $A_{ij}(t) = (\partial v_i / \partial x_j)(\mathbf{X}(t), t)$. In two dimensions, Jeffery's equation (2) can be conveniently rewritten in term of the orientation angle θ_t , defined as $\mathbf{p}(t) = (\cos \theta_t, \sin \theta_t)$, namely

$$\frac{d\theta_t}{dt} = \frac{\sigma}{2} (\cos(2\theta_t) - 1) + \frac{1}{2}\omega - \partial_x u_x \sin(2\theta_t) + \frac{1}{2}(\partial_x u_y + \partial_y u_x) \cos(2\theta_t), \quad (3)$$

where the vorticity ω and $\partial_{x,y}u$ are valued at $(\mathbf{X}(t), t)$. Using this representation actually provides additional information compared to a simple integration of (2). It indeed allows keeping track of the full unfolded angle $\theta_t \in \mathbb{R}$ rather than limiting our analysis to its folded image $\bar{\theta}_t = \arctan(p_y/p_x) \in [-\pi/2, \pi/2]$. As we will later see, this is particularly convenient when evaluating by how many turns the orientation vector \mathbf{p} has evolved over long time lags.

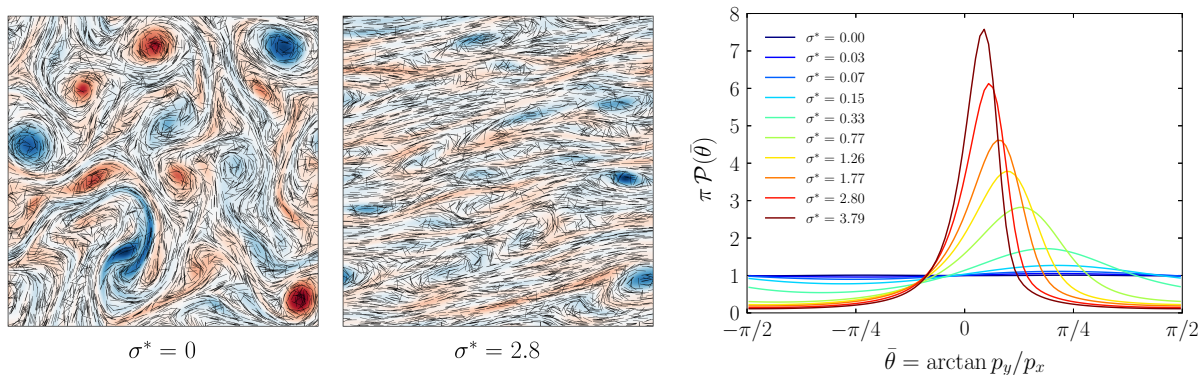


Figure 2: (Colour online) **Left:** Vorticity field $\bar{\omega}$ of the turbulent fluctuation (coloured background) for two different values of the shear rate parameter σ^* . Blue corresponds to negative values (cyclonic eddies) and red to positive values (anticyclonic). On the top of this field, the orientations of fibres are shown as black segments. **Right:** Distribution of the rods angle $\bar{\theta}_t = \arctan(p_y/p_x)$ with respect to the horizontal for various values of the shear.

In the presence of shear, rods display an anisotropic orientation and tend to preferentially align with the direction of the mean velocity gradient. This is qualitatively evidenced from the two left-hand panels of Fig. 2 that show as black segments the instantaneous direction of rods without and with shear obtained from DNS in the developed turbulent regime. In these figures, the underlying vorticity field is also shown as a coloured background. One clearly observes that rods tend in both cases to align with vorticity filaments and to experience a strong rotation when captured by vortical structures. The presence of shear causes these two type of structures to become anisotropic, filaments tending to align with a preferred angle and anticyclonic vortices (positive vorticity) being fully depleted. This has a clear impact on the rods' orientation.

To quantify this preferential alignment, we report in Fig. 2 (right) numerical measurements of the PDF of the rods folded angle $\bar{\theta}$ for various values of the shear parameter σ^* . While the distributions are almost uniform when shear is weak, they develop an increasingly concentrated peak that move towards $\bar{\theta} = 0$ when σ^* increases. The distribution of orientation can be qualitatively understood in terms of the modifications of the vorticity distribution induced by shear. The concentration of the distribution towards $\bar{\theta} = 0$ indeed results from the increasing alignment of vortex filaments with the horizontal. These results suggest that the distribution of $\bar{\theta}$ represents a direct measure of the flow anisotropies and can be used as a proxy to estimate the pitch angle of vorticity filaments with respect to the horizontal. However, estimating quantitatively such an alignment requires understanding how mean shear and turbulent fluctuations combine and compete in the orientation dynamics. Our aim is next to formulate a stochastic model for the time evolution of θ_t that accurately catches such effects.

III. A STOCHASTIC MODEL FOR RODS ORIENTATION

A. Reproducing the separation between infinitesimally close fluid elements

We propose here a Lagrangian stochastic model for the orientation dynamics of rod-like particles, with the aim to properly balance the influences of mean shear and turbulent fluctuations and the intricate interplay between spatial and temporal properties of the velocity field. The proposed approach relies on the relation between the orientation of a small, inertialess rod (infinitely thin spheroid) and the infinitesimal separation between two fluid trajectories [43]. The orientation $\mathbf{p}(t)$ that solves (2) is nothing but the normalised direction $\mathbf{p} = \mathbf{r}/|\mathbf{r}|$ of the separation vector that follows the tangent dynamics $d\mathbf{r}/dt = \mathbb{A}(t)\mathbf{r}$ along the reference tracer trajectory $\mathbf{X}(t)$. The linearity of this time evolution allows to express infinitesimal separations in terms of an evolution matrix:

$$\mathbf{r}(t) = \mathbb{D}(t, t_0) \mathbf{r}(t_0), \quad \text{with} \quad \frac{d}{dt} \mathbb{D}(t, t_0) = \mathbb{A}(t) \mathbb{D}(t, t_0) \quad \text{and} \quad \mathbb{D}(t_0, t_0) = \mathbb{1}. \quad (4)$$

The Lagrangian deformation tensor $\mathbb{D}(t, t_0)$ can be written in terms of a time-ordered matrix exponential

$$\mathbb{D}(t, t_0) = \mathcal{T} \exp \left[\int_{t_0}^t \mathbb{A}(s) ds \right] \equiv \mathbb{1} + \sum_{n=1}^{\infty} \int_{t_0}^t \int_{t_0}^{s_n} \cdots \int_{t_0}^{s_2} \mathbb{A}(s_n) \mathbb{A}(s_{n-1}) \cdots \mathbb{A}(s_1) ds_1 \cdots ds_{n-1} ds_n. \quad (5)$$

It characterises the full distortion history between times t_0 and t of infinitesimal fluid elements along the Lagrangian trajectory $\mathbf{X}(t)$. The singular values of $\mathbb{D}(t, t_0)$ describe how infinitesimal distances, areas, volumes grow under the action of fluid-velocity gradients and have been extensively studied to quantify Lagrangian chaos and turbulent mixing in the so-called Batchelor's regime [44–47]. However, when interested in the orientation statistics of small rods, relevant information is provided by the dynamics of angles and not that of amplitudes alone.

Our approach relies on the idea that an adequate model should reproduce the long-term effects of the deformation matrix (5), rather than approximating directly the Lagrangian fluid-velocity gradient \mathbb{A} . An important property of the evolution matrix is that it forms a semi-group and can thus be written as the ordered product of $N = (t - t_0)/\Delta t$ intermediate evolution matrices over an arbitrary time step Δt : $\mathbb{D}(t, t_0) = \mathbb{D}(t, t_{N-1}) \cdots \mathbb{D}(t_2, t_1) \mathbb{D}(t_1, t_0)$, where $t_n - t_{n-1} = \Delta t$. A proper statistical model for the intermediate matrices $\mathbb{D}(t_n, t_{n-1})$ ensures reproducing the long-term properties of $\mathbb{D}(t_0, t)$. This decomposition can be interpreted as a time filtering that smooths out the detailed instantaneous fluctuations of the fluid-velocity gradient \mathbb{A} . The next step consists in adequately choosing the coarse-graining time Δt with regard to the relevant timescales of the dynamics.

The first choice consists in assuming that Δt is much shorter than the inverse of the typical amplitude of \mathbb{A} , which is of the order of τ_ω (see Sec. II A). This choice allows retaining only leading terms in the time-ordered exponential

$$\mathbb{D}(t_n, t_{n-1}) = \mathbb{1} + \langle \mathbb{A} \rangle \Delta t + \int_{t_{n-1}}^{t_n} \mathbb{A}'(s) ds + \mathcal{O}(\Delta t / \tau_\omega), \quad (6)$$

where we have introduced the fluctuating fluid-velocity gradient $\mathbb{A}' \equiv \mathbb{A} - \langle \mathbb{A} \rangle$. Additionally, in order for such a model to be analytically tractable, we require that the intermediate evolution matrices be well approximated by independent Gaussian variables. This requires choosing Δt much larger than the maximal integral correlation time of the Lagrangian velocity gradient $\tau_I = \max(\tau_I^{ijkl})$ with

$$\tau_I^{ijkl} \equiv \frac{|\mathcal{I}_{ijkl}|}{\mathcal{C}_{ijij}^{1/2}(0) \mathcal{C}_{klkl}^{1/2}(0)} \quad \text{with} \quad \mathcal{I}_{ijkl} \equiv \frac{1}{2} \int_{-\infty}^{+\infty} \mathcal{C}_{ijkl}(\tau) d\tau \quad \text{and} \quad \mathcal{C}_{ijkl}(\tau) \equiv \text{cov}[\mathbb{A}_{ij}(0), \mathbb{A}_{kl}(\tau)] = \langle \mathbb{A}'_{ij}(0) \mathbb{A}'_{kl}(\tau) \rangle. \quad (7)$$

Here, summation is not assumed over repeated indices and we have used that Lagrangian velocity gradients are statistically stationary in time. Such a choice allows decomposing the integral in the right-hand side of (6) as a sum of $M = \Delta t / \tau_I \gg 1$ independent, identically distributed, random variables:

$$\int_{t_{n-1}}^{t_n} \mathbb{A}(s) ds = \sum_{m=1}^M \int_{(m-1)\tau_I}^{m\tau_I} \mathbb{A}'(t_n + s) ds \quad \text{with} \quad \left\langle \int_{(m-1)\tau_I}^{m\tau_I} \mathbb{A}'_{ij}(t_n + s) ds \int_{(m'-1)\tau_I}^{m'\tau_I} \mathbb{A}'_{kl}(t_n + s) ds \right\rangle \approx 2\tau_I \mathcal{I}_{ijkl} \delta_{m,m'}.$$

Then, applying the central-limit theorem to this sum, one gets

$$\mathbb{D}(t_n, t_{n-1}) \stackrel{\text{law}}{=} \mathbb{1} + \langle \mathbb{A} \rangle \Delta t + \mathbb{S}^{(n)} + \mathcal{O}(\Delta t / \tau_\omega) + \mathcal{O}(\Delta t / \tau_I)^{1/2}, \quad (8)$$

where the $\mathbb{S}^{(n)}$'s are Gaussian random matrices whose elements have mean and covariances

$$\langle \mathbb{S}_{ij}^{(n)} \rangle = 0, \quad \langle \mathbb{S}_{ij}^{(n)} \mathbb{S}_{kl}^{(n')} \rangle = 2\Delta t \mathcal{D}_{ijkl} \delta_{n,n'} \text{ and } \mathcal{D}_{ijkl} \approx \mathcal{I}_{ijkl}. \quad (9)$$

Before extending further this approach, let us briefly comment on its validity. The proposed model relies on two assumptions: The first, $\Delta t \ll \tau_\omega$, allows to consider only the leading term of the time-ordered exponential (5); The second, $\Delta t \gg \tau_\Gamma$, consists in assuming that scales at which we observe the system are much longer than the correlation time of the fluid-velocity gradients, allowing to assume Gaussian statistics for not-too-large fluctuations. Finding out an adequate coarse-graining time scale Δt such that $\tau_\Gamma \ll \Delta t \ll \tau_\omega$ requires a sufficient scale separation that is ensured by a small value of the *Kubo number* $\text{Ku} = \tau_\Gamma/\tau_\omega \ll 1$. This quantity is a dimensionless measurement of the Lagrangian correlation time with respect to the typical amplitude of velocity gradients. In three-dimensional turbulent flow, this number is known to be at least of the order of one. As we will later see (Sec. III C), the absence of vortex stretching and the presence of long-standing structures in two dimensions are responsible for observing rather large values of Ku . For that reason, we keep free how to select the covariance tensor \mathcal{D}_{ijkl} in order to compare different alternatives. Nevertheless and in spite of the apparent inconsistency of the proposed approach, we will see in next section that the choice $\mathcal{D}_{ijkl} = \mathcal{I}_{ijkl}$ fairly reproduces low-order statistics for the orientation of rod particles.

The next step in our approach consists in finding out the evolution equation that is satisfied by a stochastic effective separation $\mathbf{r}^*(t)$ whose statistics will reproduce those of the original infinitesimal separation $\mathbf{r}(t)$. As it is often the case in stochastic modelling, there is an ambiguity on how to interpret the multiplicative noise that appears in the stochastic differential equation (SDE) followed by \mathbf{r}^* . The choice between Itô and Stratonovich interpretations is here settled by the idea that the evolution matrix associated to the model dynamics should reproduce, to leading order, the right-hand side of Eq. (8). Using generalisations of the time-ordered exponential series (5) to the case of SDEs [48], we find that the appropriate interpretation is Stratonovich's. The evolution equation for $\mathbf{r}^*(t)$ is then recovered by replacing Eq. (8) into Eq. (4), leading to

$$d\mathbf{r}^* = \langle \mathbb{A} \rangle \mathbf{r}^* dt + (\mathbb{B} \partial \mathbb{W}_t) \mathbf{r}^*. \quad (10)$$

Here, \mathbb{B} is a deterministic tensor such that $\mathbb{B}_{ijmn} \mathbb{B}_{klmn} = 2 \mathcal{D}_{ijkl}$, the $d \times d$ random matrix \mathbb{W} is made of independent Brownian motions, d denoting the space dimension, and the differential ∂ emphasises that the stochastic integral has to be interpreted in Stratonovich's sense. A statistical model $\mathbf{p}^*(t)$ for the orientation vector of rod particles in two-dimensional homogeneous shear flow is then obtained by prescribing $d = 2$, that $\langle \mathbb{A}_{ij} \rangle = \sigma \delta_{i,1} \delta_{j,2}$ and by normalising the separation vector solution of Eq. (10) by its length, *i.e.* $\mathbf{p}^*(t) = \mathbf{r}^*(t)/|\mathbf{r}^*(t)|$, as in the deterministic case. Note that the considerations leading to such a model are valid in any spatial dimension d .

Quantitative comparisons between the statistical model for the orientation $\mathbf{p}(t)$ and the results of DNS require properly matching timescales. In the above model, the relative importance of the average gradient compared to its fluctuations is measured through the ratio $\sigma/\|\mathcal{D}\|$, which balances the mean shear to a norm of the correlation tensor \mathcal{D}_{ijkl} and thus, in principle, to the long-term Lagrangian statistics of fluid-velocity gradients. However, we have seen in Sec. II A that the relevant way to non-dimensionalise the results of DNS is to introduce the turnover time τ_ω , defined as the inverse of the root-mean-squared vorticity, and thus to measure the relative importance of mean shear through the dimensionless parameter $\sigma^* = \tau_\omega \sigma$. Matching the model to DNS thus requires calibrating the correlation amplitude $\|\mathcal{D}\|$ in units of τ_ω . This will be done by introducing an adjustable dimensionless multiplicative parameter.

B. An effective stochastic model over angles

We here turn back to the two-dimensional case to write, in a similar way to the deterministic dynamics (3), a stochastic model equation for the evolution of the folded orientation angle $\bar{\theta}_t \equiv \arctan(p_y^*(t)/p_x^*(t)) = \arctan(r_y^*(t)/r_x^*(t))$ with values in $[-\pi/2, \pi/2]$. Note that, in the sake of simplifying notations, we dropped here the $*$ symbol used to refer to statistically modelled quantities. Applying the Itô formula to Eq. (10) (see Appendix A), $\bar{\theta}_t$ is found to follow

$$\bar{\theta}_t = \text{cmod} \left(\bar{\theta}_0 + \int_0^t a(\bar{\theta}_s) ds + \int_0^t b(\bar{\theta}_s) \partial W_s \right), \quad (11)$$

where W_t is a one-dimensional Brownian motion, $\text{cmod}(x) := ((x + \pi/2) \bmod \pi) - \pi/2$, and the stochastic integral is again understood with the Stratonovich convention. The drift and diffusion coefficients are respectively,

$$a(\bar{\theta}) = \frac{\sigma^*}{2} (\cos(2\bar{\theta}) - 1), \quad b(\bar{\theta}) = (\gamma_0 + \gamma_1 \sin(2\bar{\theta}) + \gamma_2 \sin(4\bar{\theta}) + \gamma_3 \cos(2\bar{\theta}) + \gamma_4 \cos(4\bar{\theta}))^{1/2}. \quad (12)$$

The γ_n parameters are expressed in terms of the effective diffusion tensor \mathcal{D}_{ijkl} appearing in (10) through

$$\begin{aligned}\gamma_0 &= \mathcal{D}_{1111} + \frac{1}{2} \mathcal{D}_{1221} + \frac{3}{4} (\mathcal{D}_{2121} + \mathcal{D}_{1212}), & \gamma_1 &= 2 (\mathcal{D}_{1112} - \mathcal{D}_{1121}), \\ \gamma_2 &= -\mathcal{D}_{1112} - \mathcal{D}_{1121}, & \gamma_3 &= \mathcal{D}_{2121} - \mathcal{D}_{1212}, \\ \gamma_4 &= -\mathcal{D}_{1111} + \frac{1}{2} \mathcal{D}_{1221} + \frac{1}{4} (\mathcal{D}_{2121} + \mathcal{D}_{1212}).\end{aligned}\quad (13)$$

It is important to notice that the model (11)-(12) for orientation dynamics involves diffusive terms that are proportional to $\cos(4\bar{\theta})$ and $\sin(4\bar{\theta})$, in contrast with its deterministic, smooth counterpart of Sec. II B. This is a consequence of the projection of the diffusive dynamics of $\mathbf{r}^*(t)$ onto the unit sphere and such terms would not have been present if the model had been directly derived from the physical angle dynamics (3). The considerations of previous section however show that our approach is a consistent manner to consider the cumulative effects of the fluid-velocity gradient.

In view of comparing the statistical model to DNS, we first focus on the stationary distribution of rod orientations. The probability density function $\mathcal{P}(\bar{\theta}, t)$ of the stochastic folded angle satisfies the Fokker–Planck equation

$$\partial_t \mathcal{P}(\bar{\theta}, t) + \partial_{\bar{\theta}} j(\bar{\theta}, t) = 0, \quad (14)$$

where the *probability current*, which represents the amount of probability flux across a given point $\bar{\theta}$, reads

$$j(\bar{\theta}, t) \equiv a(\bar{\theta}) \mathcal{P}(\bar{\theta}, t) - \frac{1}{2} b(\bar{\theta}) \partial_{\bar{\theta}} [b(\bar{\theta}) \mathcal{P}(\bar{\theta}, t)]. \quad (15)$$

The Fokker–Planck equation (14) is supplemented with periodic boundary conditions $\mathcal{P}(-\pi/2, t) = \mathcal{P}(\pi/2, t)$, and the usual normalisation of the probability density function $\int_{-\pi/2}^{\pi/2} \mathcal{P}(\bar{\theta}, t) d\bar{\theta} = 1$.

It has been shown in [49] that the process $\bar{\theta}_t$ is an ergodic diffusion, ensuring that its distribution reaches at long times a uniquely defined statistical steady state given by a stationary solution $\mathcal{P}_{\text{st}}(\bar{\theta})$ of (14). This solution corresponds to a constant probability current, $j(\bar{\theta}, t) = -\mathcal{J}$, and satisfies

$$\partial_{\bar{\theta}} [b(\bar{\theta}) \mathcal{P}_{\text{st}}(\bar{\theta})] = \frac{2a(\bar{\theta})}{b(\bar{\theta})} \mathcal{P}_{\text{st}}(\bar{\theta}) + \frac{2\mathcal{J}}{b(\bar{\theta})}. \quad (16)$$

It is important to notice that such a solution exists only if the diffusion coefficient $b(\bar{\theta})$ never vanishes. This has been verified numerically for the various values of the γ_n 's parameters used in this study (see Appendix B). Integrating (16) leads to

$$\mathcal{P}_{\text{st}}(\bar{\theta}) = \frac{e^{\Psi(\bar{\theta})}}{\mathcal{N} b(\bar{\theta})} \left(1 + 2\mathcal{J} \mathcal{N} \int_{-\pi/2}^{\bar{\theta}} \frac{e^{-\Psi(\bar{\theta}')}}{b(\bar{\theta}')} d\bar{\theta}' \right), \quad \text{with} \quad \Psi(\bar{\theta}) = \int_{-\pi/2}^{\bar{\theta}} \frac{2a(\bar{\theta}')}{b^2(\bar{\theta}')} d\bar{\theta}', \quad (17)$$

$$\text{and} \quad \mathcal{N} = \left[\int_{-\pi/2}^{\pi/2} \frac{e^{\Psi(\bar{\theta})}}{b(\bar{\theta})} d\bar{\theta} \right] \left[1 - 2\mathcal{J} \int_{-\pi/2}^{\pi/2} \frac{e^{\Psi(\bar{\theta})}}{b(\bar{\theta})} \int_{-\pi/2}^{\bar{\theta}} \frac{e^{-\Psi(\bar{\theta}')}}{b(\bar{\theta}')} d\bar{\theta}' d\bar{\theta} \right]^{-1}. \quad (18)$$

The constant \mathcal{N} ensures here the normalisation of \mathcal{P}_{st} . The probability current \mathcal{J} is obtained by imposing periodic boundary conditions: $\mathcal{P}_{\text{st}}(\pi/2) = \mathcal{P}_{\text{st}}(-\pi/2)$. This leads to

$$\mathcal{J} = \frac{1}{2} \left[\frac{1}{e^{-\Psi(\pi/2)} - 1} \int_{-\pi/2}^{\pi/2} \frac{e^{\Psi(\bar{\theta})}}{b(\bar{\theta})} d\bar{\theta} \int_{-\pi/2}^{\pi/2} \frac{e^{-\Psi(\bar{\theta})}}{b(\bar{\theta})} d\bar{\theta} + \int_{-\pi/2}^{\pi/2} \frac{e^{\Psi(\bar{\theta})}}{b(\bar{\theta})} \int_{-\pi/2}^{\bar{\theta}} \frac{e^{-\Psi(\bar{\theta}')}}{b(\bar{\theta}')} d\bar{\theta}' d\bar{\theta} \right]^{-1}. \quad (19)$$

C. Comparison of different models for the correlation tensor

To contrast the above analytical stationary distribution with the result of DNS, we need to prescribe the effective correlation tensor \mathcal{D}_{ijkl} that enters the definitions (12)-(13) of the model diffusion coefficient b . We consider and compare three different choices, with an increasing level of complexity.

The first case, which is the most straightforward, consists in assuming that fluctuations are isotropic. Together with the incompressibility constraint, this leads to write the effective correlation tensor as

$$\mathcal{D}_{ijkl} \approx \mathcal{D}_{ijkl}^{\text{iso}} \equiv \frac{\alpha_{\text{iso}}}{\tau_{\omega}} (3\delta_{ik}\delta_{jl} - \delta_{ij}\delta_{kl} - \delta_{il}\delta_{jk}). \quad (20)$$

This approximation follows most common approaches in statistical models of Lagrangian turbulence. The parameter α_{iso} is often interpreted as a Kubo number and links the instantaneous properties of the flow (entailed in τ_{ω}) to

the long-term effect of gradients that the noise with correlations \mathcal{D}_{ijkl} is expected to reproduce. In that case, noise correlations are independent of the mean shear σ^* . Also, when using such a form, the stochastic model of previous subsection is drastically simplified: all γ_n 's except γ_0 vanish in the diffusion coefficient (12).

The second case that we investigate consists in accounting for the single-time anisotropies of the fluid-velocity gradients that are caused by the mean shear. The effective correlation tensor then reads

$$\mathcal{D}_{ijkl} \approx \mathcal{D}_{ijkl}^{\text{aniso}} \equiv \alpha_{\text{aniso}} \tau_\omega \mathcal{C}_{ijkl}(0), \quad (21)$$

where, as previously, α_{aniso} is a calibration parameter that can be interpreted as a Kubo number. $\mathcal{C}_{ijkl}(0)$ is here the equal-time covariance matrix of the fluid-velocity gradients, as defined in Eq. (7). We then rely on DNS data to evaluate how this correlation tensor depends on the mean shear. The six independent components of $\mathcal{C}_{ijkl}(0)$ are shown in Fig. 3 (left) as a function of σ^* . Most important deviations from isotropy occur both for the component along the mean shear $\mathcal{C}_{1212}(0) = \langle (\partial_y u_x)^2 \rangle$, which increases as a function of σ^* , and for the transverse component $\mathcal{C}_{2121}(0) = \langle (\partial_x u_y)^2 \rangle$, which is depleted by shear.

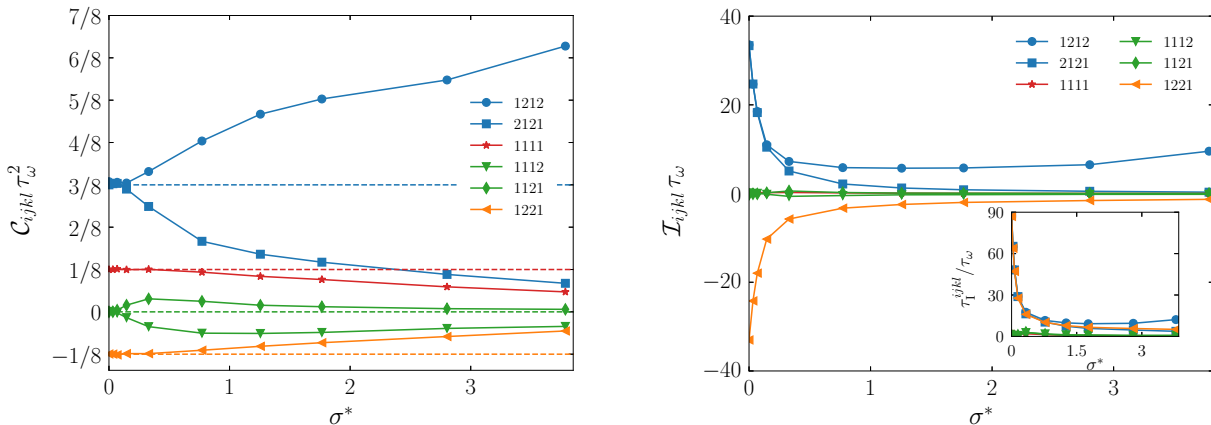


Figure 3: (Colour online) **Left:** One-point, one-time correlation $\mathcal{C}_{ijkl}(0)$ of the fluid-velocity gradient tensor obtained from DNS, as a function of the dimensionless shear parameter $\sigma^* = \tau_\omega \sigma$, where $\tau_\omega = \langle \omega^2 \rangle^{-1/2}$. The horizontal dashed lines correspond to isotropic statistics. **Right:** Integral correlation tensor \mathcal{I}_{ijkl} measured as in Eq. (7) as a function of σ^* . The inset shows the corresponding component-dependent Lagrangian integral correlation time τ_1^{ijkl} .

Finally, the third case follows the considerations of Sec. III A in order to better approximate the cumulative effects of the velocity gradient along Lagrangian paths. The noise correlations here reads

$$\mathcal{D}_{ijkl} \approx \mathcal{D}_{ijkl}^{\text{int}} \equiv \alpha_{\text{int}} \mathcal{I}_{ijkl}, \quad (22)$$

where \mathcal{I}_{ijkl} denotes the time-integral of the two-time Lagrangian covariance of the velocity gradient tensor and was defined in Eq. (7). In the same spirit as before, a tuning parameter α_{int} is introduced. This time, however, the dependence on correlation times is entailed in the definition of \mathcal{I}_{ijkl} , so that α_{int} cannot be straightforwardly assimilated to a Kubo number. As discussed in Sec. III A it rather parametrises the relationship between single-time and averages fluctuations and depends, in principle, on the details of the underlying coarse-graining procedure. The six independent components of the integral tensor \mathcal{I}_{ijkl} measured from DNS are shown in Fig. 3 (right). At $\sigma^* = 0$, transverse components are markedly large, which is a very strong signature of the presence of long-living rotating structures in the flow. One observes there that $\mathcal{I}_{1212} = \mathcal{I}_{2121} = -\mathcal{I}_{1221}$, confirming the strongly circular Beltrami nature of the vortices. The measured values indicate that tracers typically spend tens of turnover times in such structures. The effect of increasing σ^* is to rapidly reduce such correlations, a signature of the depletion of structures by shear (see Sec. II A). At larger values $\sigma^* \gtrsim 0.15$, anisotropies start to develop, in particular for the component \mathcal{I}_{1212} along the mean shear direction. Clearly, the behaviour of the integral correlations \mathcal{I}_{ijkl} is very different from the single-time correlations $\mathcal{C}_{ijkl}(0)$ shown on the left-hand figure. Obviously, the two correlations are not related by a simple proportionality law. To assess the peculiar behaviour of Ku in two dimensional turbulence, the corresponding component-dependent are displayed in inset of Fig. 3 (right).

The results of the three models are balanced and contrasted to DNS data. To make this tractable, we focus on the stationary distribution \mathcal{P}_{st} of the folded orientation angle and on its mean value $\langle \hat{\theta} \rangle = \int \hat{\theta} \mathcal{P}_{\text{st}}(\hat{\theta}) d\hat{\theta}$. Different values

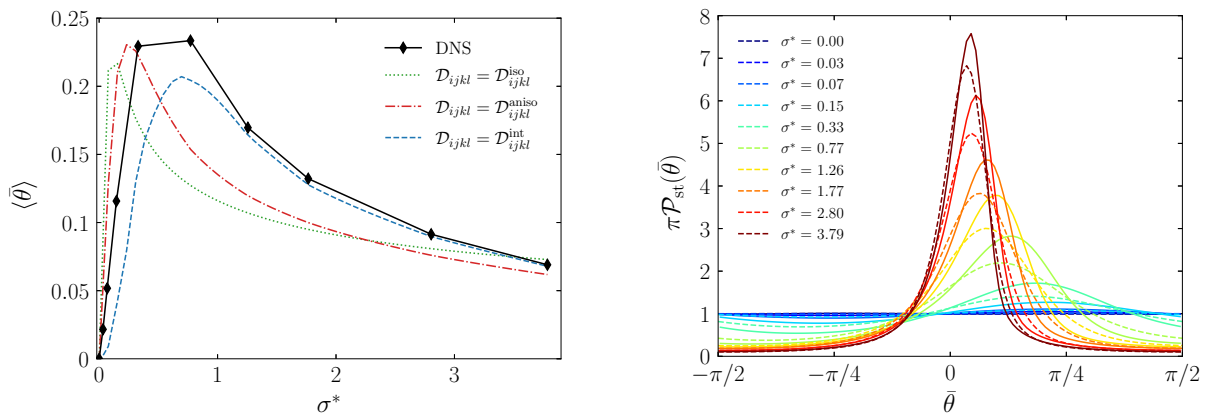


Figure 4: (Colour online) **Left:** Variation as a function of σ^* of the average orientation angle $\langle \bar{\theta} \rangle$ obtained from the DNS and the three models, as labeled. The three selected parameters were $\alpha_{iso} = 0.076$, $\alpha_{aniso} = 0.189$, and $\alpha_{int} = 0.053$. **Right:** Stationary distribution \mathcal{P}_{st} of the rods folded angle obtained with the integral correlation tensor \mathcal{D}_{ijkl}^{int} with $\alpha_{int} = 0.053$ and for various values of the shear (dashed lines). DNS measurements for different values of σ^* are shown as continuous lines.

of the free parameters α_{iso} , α_{aniso} , and α_{int} have been tested to minimise errors, not only in terms of $\langle \bar{\theta} \rangle$, but also for the peak of the stationary orientation distribution.

The results obtained with the isotropic correlation \mathcal{D}_{ijkl}^{iso} reproduce the DNS, only for small values of σ^* . When the shear rate increases, the stationary distribution becomes less peaked than the DNS (not shown), even for the optimal value $\alpha_{iso} = 0.076$. This behaviour is confirmed in Fig. 4 (left), which represents $\langle \bar{\theta} \rangle$ as a function of the shear rate. Discrepancies are important for all finite values of σ^* . The anisotropic model is thus found to have a limited effectiveness to reproduce DNS statistics, even at a qualitative level.

When using the anisotropic tensor $\mathcal{D}_{ijkl}^{aniso}$, the stationary distribution \mathcal{P}_{st} is in better agreement with DNS. The average value $\bar{\theta}$ shown in Fig. 4 (left) displays clear improvements with respect to the isotropic model, in particular for large values of the shear rate. Still, this anisotropic model based on single-time gradients statistics reproduces only the trends that the presence of shear produces in the DNS. Its effectiveness is restricted to qualitative aspects.

Quantitative agreements between the model and the simulations are obtained when using the integral correlation tensor \mathcal{D}_{ijkl}^{int} . This is clear for the average angle shown in Fig. 4 (left), in particular at large values of the shear parameter. Discrepancies can only be appreciated at intermediate values of σ^* , for which the model angular distribution is noticeably less peaked than in DNS. This can be seen in Fig. 4 (right), which shows the stationary distribution \mathcal{P}_{st} of the rods angle both for the model with integral correlations and for DNS data. The agreement is the greatest at the largest values of σ^* . This can be qualitatively explained. As discussed in Sec. III A, modelling the fluid-velocity gradient in terms of a white-noise with correlations \mathcal{D}_{ijkl}^{int} requires a small Kubo number, and thus typical correlation times shorter than the turnover time τ_w . A strong shear is responsible for a shortening of the living time of coherent structures and thus of a decrease of correlation times that becomes of the same order as the shear timescale σ^{-1} (see the inset of Fig. 3 right). We thus expect that $Ku < 1/\sigma^*$, so that the white-noise limit could be asymptotically reached in the limit of strong shear.

Above results on single-time stationary statistics for the orientation of rods suggest that the model (22) based on integral correlations gives the best approximation of velocity gradient fluctuations. We hereafter concentrate on it and we next investigate its effectiveness for two-time statistics.

IV. TUMBLING STATISTICS

In situations where the average velocity gradient vanishes, the angular dynamics of non-spherical particles is usually measured in terms of the *tumbling rate*, which is defined as the root-mean-squared rate of change $\langle |d\mathbf{p}/dt|^2 \rangle^{1/2}$ of the orientation vector. Much numerical and experimental work has focused on tumbling rate statistics (see [20] for a review). However, in the framework of stochastic Lagrangian models, the orientation vector \mathbf{p} diffuses, preventing from properly defining the tumbling rate. Nevertheless, alternative quantities can be introduced in order to gain access to fluctuations of the rods rotation rates and to provide quantitative predictions.

Our idea consists in unfolding the orientation angle $\bar{\theta}_t \in [-\pi/2, \pi/2]$ to the whole real line, and to investigate the

long-term evolution of the rods orientation in terms of the (non-stationary) dynamics of the unfolded angle $\theta_t \in \mathbb{R}$. This evolution is entailed in the angular displacement $\delta\theta_t = \theta_t - \theta_0$ that represents the change in time of the unfolded angle with respect to its initial position. In its classical definition, the tumbling rate describes the instantaneous rate of change of the orientation and enters the short-time evolution of the angular displacement: A Taylor expansion indeed gives $\langle \delta\theta_t^2 \rangle \approx t^2 \langle |d\mathbf{p}/dt|^2 \rangle$. At extremely long times, the angular displacement is expected to reach a diffusive regime where the variance of $\delta\theta_t$ grows linearly with time. The stochastic model for rods orientation that was introduced in previous section should capture this ultimate behaviour.

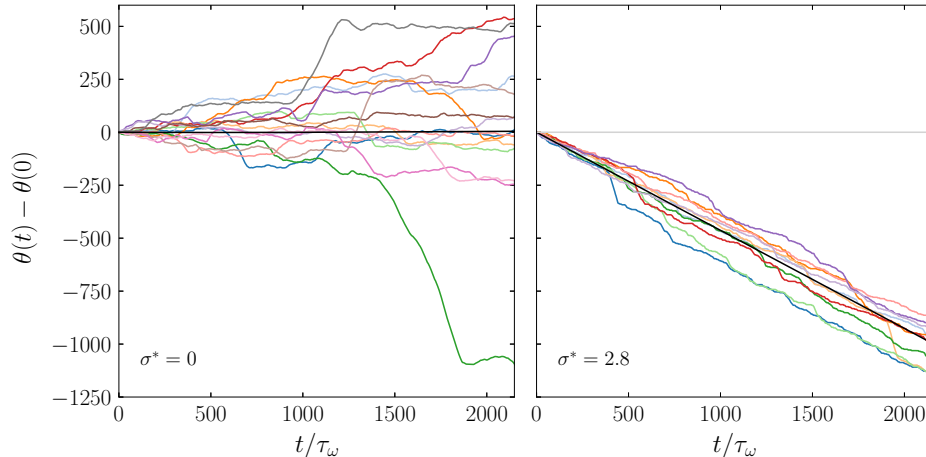


Figure 5: (Colour online) Typical trajectories of the angular displacement $\delta\theta_t = \theta_t - \theta_0$ obtained from DNS in the absence of shear (left panel) and for $\sigma^* = 2.8$ (right panel). Their average behaviour is shown as black lines.

Figure 5 shows several trajectories of the angular displacement extracted from DNS. In the absence of shear $\sigma^* = 0$ (left-hand panel), rod orientations fluctuate along their mean $\langle \theta_t \rangle = \theta_0$. Still, one qualitatively observes that at intermediate times, angular fluctuations can probably not be described in terms of a simple diffusion, because they involve strong quasi-ballistic excursions during which $\delta\theta_t$ varies linearly. This corresponds to events during which Lagrangian tracers are captured by vortex structures and, as we will see later, these long-range excursions resembles the behaviour of Lévy walks. In the presence of a mean shear $\sigma^* > 0$ (right-hand panel), the average angular displacement $\langle \delta\theta_t \rangle$ decreases linearly as a function of time. This is a signature of the out-of-equilibrium dynamics reached by the folded orientation angle. Indeed, when $\sigma^* \rightarrow \infty$, the rod orientation has a fixed point at $\bar{\theta} = 0$ (*i.e.* $\theta = 0 \bmod \pi$), where the local dynamics follows $d\bar{\theta}/dt \approx -\sigma^* \bar{\theta}^2$. This fixed point attracts in a finite time all trajectories approaching it from $\bar{\theta} > 0$, but any perturbation that pushes the orientation angle to $\bar{\theta} < 0$ triggers an instability and the rod initiates a Jeffery orbit. At finite values of σ^* , the fluctuations of velocity gradients are perturbing this quasi-equilibrium causing the rod to frequently tumble. In the stochastic model of previous section, this average angular displacement is entailed in the constant negative probability current $-\mathcal{J}$ that characterises the stationary distribution of the folded angle $\bar{\theta}_t$. DNS results moreover show that ballistic excursions of $\delta\theta_t$ are also present in the case with shear, but this time with a negative bias reflecting the skewness of the vorticity distribution.

As we will now see, such considerations lead to introduce two different measures for the rod tumbling rate: one reflecting the effect of a mean shear and obtained from the average angular displacement $\delta\theta_t$; the other associated to the long-time diffusive behaviour of $\delta\theta_t$ and obtained from its variance.

A. Average angular displacement

Using known properties of diffusions on the torus [49], one can show that the unfolded orientation angle $\theta_t \in \mathbb{R}$ associated to the stochastic model (11) follows exactly the same stochastic differential equation as its folded counterpart, but this time on \mathbb{R} rather than on the periodic domain $[-\pi/2, \pi/2]$. One can thus write

$$\delta\theta_t = \theta_t - \theta_0 = \int_0^t a(\theta_s) ds + \int_0^t b(\theta_s) \partial W_s, \quad (23)$$

where W_t is the exact same realisation of the Brownian motion as that entering the time evolution of $\bar{\theta}_t$. The drift and diffusion coefficients a and b , defined in (12) are periodic functions of θ_t . It thus makes no difference evaluating

them along the folded process $\bar{\theta}_t = \theta_t \bmod \pi$. For a sake of simplicity, let us assume that the initial orientation angle θ_0 is chosen in $[-\pi/2, \pi/2]$, with a distribution given by the stationary solution \mathcal{P}_{st} to the Fokker–Planck equation (16). This means that at any later time $t > 0$, the folded angle $\bar{\theta}_t$ remains distributed according to the stationary law. We then use Itô’s formulation of Eq. (23) to write its average as

$$\langle \delta\theta_t \rangle = \int_0^t \left\langle a(\bar{\theta}_s) + \frac{1}{4} \partial_{\bar{\theta}} b^2(\bar{\theta}_s) \right\rangle ds = t \left\langle a(\bar{\theta}) + \frac{1}{4} \partial_{\bar{\theta}} b^2(\bar{\theta}) \right\rangle. \quad (24)$$

To simplify notations, expectations involving $\bar{\theta}$ are, here and in the sequel, understood as averages over the stationary distribution, and $\langle a(\bar{\theta}) + \frac{1}{4} \partial_{\bar{\theta}} b^2(\bar{\theta}) \rangle \equiv \int_{-\pi/2}^{\pi/2} [a(\bar{\theta}) + \frac{1}{4} \partial_{\bar{\theta}} b^2(\bar{\theta}_s)] \mathcal{P}_{\text{st}}(\bar{\theta}) d\bar{\theta} = -\pi \mathcal{J}$. We finally obtain that the average tumbling rate reads

$$\dot{\theta}_{\infty} \equiv \frac{d}{dt} \langle \delta\theta_t \rangle = -\pi \mathcal{J}. \quad (25)$$

Figure 6 (left) shows the time evolution of average angular displacements, both for the DNS (solid lines) and for the stochastic model with integral correlations (dashed lines), at various values of the mean shear rate. For the model, the tuning parameter was chosen to be $\alpha_{\text{int}} = 0.053$, corresponding to the optimal choice to reproduce both the average and the stationary distribution of the folded angle $\bar{\theta}$ (see Sec. III C). In both cases, the average angular displacement is zero when $\sigma^* = 0$ and becomes increasingly negative when σ^* increases. For this specific choice of the parameter α_{int} , the model shows discrepancies with respect to DNS that are of the order of 20% of the mean angular velocity $\dot{\theta}_{\infty}$ at the largest values of σ^* .

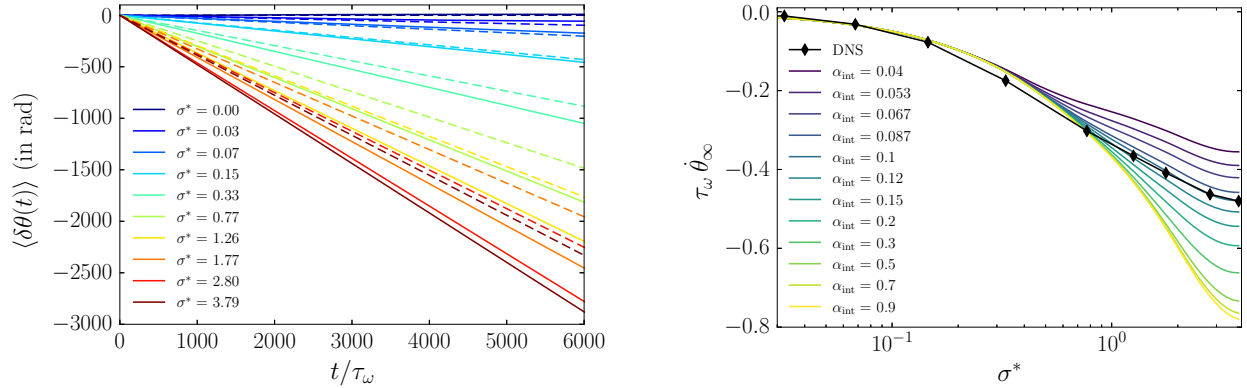


Figure 6: (Colour online) **Left:** Average angular displacement of the unfolded angle $\delta\theta_t = \theta_t - \theta_0$ as a function of time for various values of shear rate σ^* , showing a linear behaviour $\langle \delta\theta_t \rangle \simeq \dot{\theta}_{\infty} t$ at long times. DNS results are represented as solid lines and model values as dashed lines (here for $\alpha_{\text{int}} = 0.053$). **Right:** Asymptotic angular velocity $\dot{\theta}_{\infty}$ as a function of the shear rate parameter σ^* from DNS (\blacklozenge) and the model (coloured lines) for various values of α_{int} , as labelled.

In order to better assess the dependence upon the tuning parameter α_{int} of the model, we show in the right-hand panel of Fig. (6) how the average tumbling rate $\dot{\theta}_{\infty}$ changes when varying α_{int} over an extended range. DNS results are also shown as symbols and we find that the best match is obtained for $\alpha_{\text{int}} \approx 0.1$, a value that is roughly twice larger than that used to fit the stationary distribution in Sec. III C. This necessity to increase significantly the tuning parameter, and consequently the strength of diffusion in the stochastic model, can be again interpreted as a signature of the coherent structures that are present in the actual turbulent flow. For the stochastic model, the probability current, and consequently the average tumbling, only depends on how the degenerate stable fixed point $\bar{\theta} = 0$ is instantaneously perturbed. In the turbulent flow, $\bar{\theta} = 0$ is no more a fixed point for tracers that are captured in the persistent structures with a positive vorticity. They contribute to an increase of the average tumbling rate, but at the same time, they tend to uniformise the distribution of the folded angle. These two effects cannot be simultaneously captured by the stochastic model. They can only be reproduced individually using different values of the tuning parameter α_{int} . Still, it is worth emphasising that, a single adjustment of α_{int} makes the model reproduce the tumbling rate $\dot{\theta}_{\infty}$ for all values of the shearing rates σ^* that we considered.

B. Variance of angular displacement

The long-time diffusive behaviour of the orientation angle leads to introduce another tumbling rate, defined as the asymptotic growth rate of the variance of the angular displacement

$$\mathcal{D}_{\sigma^*} = \lim_{t \rightarrow \infty} \frac{d}{dt} \left\langle (\delta\theta_t - \langle \delta\theta_t \rangle)^2 \right\rangle. \quad (26)$$

The analytical estimation of this diffusion coefficient, and thus of second-order statistics of the unfolded orientation angle θ_t , is much less trivial than the calculation of the average angular displacement reported in previous subsection. The first step consists in writing the second-order moment of the angular displacement as

$$\left\langle (\delta\theta_t - \langle \delta\theta_t \rangle)^2 \right\rangle = \left\langle \left[\int_0^t (\widehat{a}(\bar{\theta}_s) - \langle \widehat{a}(\bar{\theta}) \rangle) ds \right]^2 \right\rangle + \left\langle \int_0^t b^2(\bar{\theta}_s) ds \right\rangle,$$

where $\widehat{a}(\theta) = a(\theta) + \frac{1}{4} \partial_\theta b^2(\theta)$ denotes the Itô version of the model drift in (23). As in previous subsection, here again we assume that θ_0 is chosen in $[-\pi/2, \pi/2]$ according to the stationary law \mathcal{P}_{st} , and thus that the folded process $\bar{\theta}_t$ follows \mathcal{P}_{st} at any later time. This allows us writing

$$\frac{d}{dt} \left\langle (\delta\theta_t - \langle \delta\theta_t \rangle)^2 \right\rangle = 2 \left\langle \widehat{a}(\bar{\theta}_0) \int_0^t [\widehat{a}(\bar{\theta}_s) - \langle \widehat{a}(\bar{\theta}) \rangle] ds \right\rangle + \langle b^2(\bar{\theta}) \rangle. \quad (27)$$

To evaluate the first term on the right-hand side, we employ a useful method involving the auxiliary Poisson equation with an appropriate source term [50]. Let us consider η solution for $\theta \in [-\pi/2, \pi/2]$ of

$$\frac{1}{2} b^2(\theta) \partial_\theta^2 \eta(\theta) + \widehat{a}(\theta) \partial_\theta \eta(\theta) = \widehat{a}(\theta) - \langle \widehat{a}(\bar{\theta}) \rangle, \quad \text{with } \partial_\theta \eta(-\pi/2) = \partial_\theta \eta(\pi/2). \quad (28)$$

By Integrating (28) against \mathcal{P}_{st} and using the Fokker–Planck equation (16) for \mathcal{P}_{st} , one can show that the solution η must be periodic as well. Applying the Itô formula to $\eta(\bar{\theta}_t)$, evaluated along the folded process, we moreover get

$$\begin{aligned} \eta(\bar{\theta}_t) - \eta(\bar{\theta}_0) &= \int_0^t \left[\widehat{a}(\bar{\theta}_s) \partial_\theta \eta(\bar{\theta}_s) + \frac{1}{2} b^2(\bar{\theta}_s) \widehat{a}(\bar{\theta}_s) \partial_\theta^2 \eta(\bar{\theta}_s) \right] ds + \int_0^t \partial_\theta \eta(\bar{\theta}_s) b(\bar{\theta}_s) dW_s \\ &= \int_0^t [\widehat{a}(\bar{\theta}_s) - \langle \widehat{a}(\bar{\theta}) \rangle] ds + \int_0^t \partial_\theta \eta(\bar{\theta}_s) b(\bar{\theta}_s) dW_s, \end{aligned}$$

where, for the second equality, we used that η solves the Poisson equation (28). Multiplying by $\widehat{a}(\bar{\theta}_0)$ and averaging with respect to noise, the contribution from the stochastic integral vanishes and

$$\left\langle \widehat{a}(\bar{\theta}_0) \int_0^t [\widehat{a}(\bar{\theta}_s) - \langle \widehat{a}(\bar{\theta}) \rangle] ds \right\rangle = \langle \widehat{a}(\bar{\theta}_0) \eta(\bar{\theta}_t) \rangle - \langle \widehat{a}(\bar{\theta}) \eta(\bar{\theta}) \rangle.$$

When $t \rightarrow \infty$, the first term de-correlates to approach $\langle \widehat{a}(\bar{\theta}_0) \rangle \langle \eta(\bar{\theta}_t) \rangle$. Using both the Poisson equation for η and the Fokker–Planck equation for \mathcal{P}_{st} , one can show that $2 \langle \widehat{a}(\bar{\theta}) \rangle \langle \eta(\bar{\theta}) \rangle - 2 \langle \widehat{a}(\bar{\theta}) \eta(\bar{\theta}) \rangle = \langle b^2(\bar{\theta}) (\partial_\theta \eta)^2(\bar{\theta}) \rangle$. Putting together the two contributions of (27), we finally find that the diffusion coefficient (26) reads

$$\mathcal{D}_{\sigma^*} = \langle b^2(\bar{\theta}) \rangle + \langle b^2(\bar{\theta}) (\partial_\theta \eta)^2(\bar{\theta}) \rangle, \quad (29)$$

where we recall that averages involving $\bar{\theta}$ are taken with respect to the stationary distribution \mathcal{P}_{st} . This expression can be handle with precision using the semi-explicit solution of the Poisson equation: With the same notation $\Psi(\theta)$ involved in the definition of the stationary distribution \mathcal{P}_{st} in (17), one has

$$\partial_\theta \eta(\theta) = 1 - 2\pi \mathcal{J} \frac{e^{-\Psi(\theta)}}{b(\theta)} \left(\frac{\int_{-\pi/2}^{\pi/2} \frac{e^{-\Psi(\theta')}}{b(\theta')} d\theta'}{1 - e^{-\Psi(\pi/2)}} - \int_{-\pi/2}^{\theta} \frac{e^{-\Psi(\theta')}}{b(\theta')} d\theta' \right). \quad (30)$$

Note that when $\sigma^* \rightarrow 0$, the source term $\langle \widehat{a}(\bar{\theta}) \rangle$ vanishes and the solution of (28) is trivially $\partial_\theta \eta(\theta) \equiv 1$.

Figure 7 (left) shows DNS measurements of the variance of the angular increment $\delta\theta_t$ as a function of time. After a ballistic regime at very short times, there is a transition zone at intermediate times where the behaviour is possibly

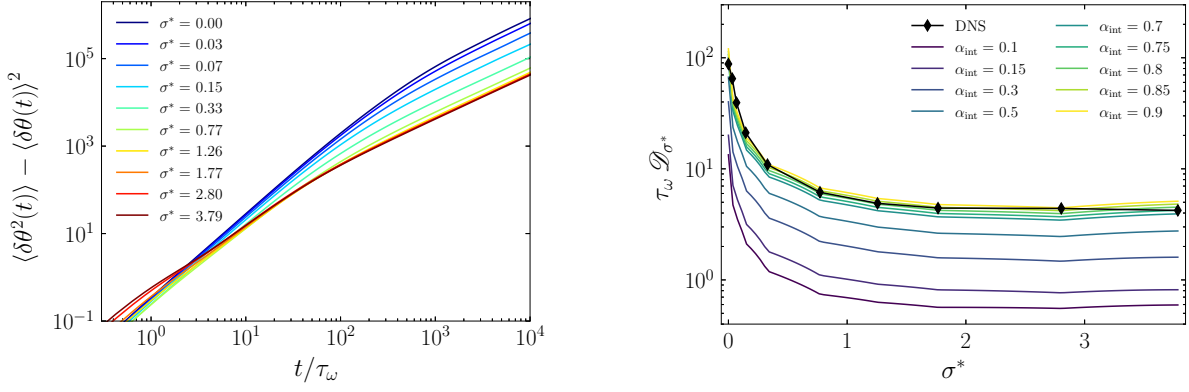


Figure 7: (Colour online) **Left:** Variance of the angular increment $\delta\theta_t$ as a function of time measured from DNS for various values of the shear rate. Data show a diffusive regime for $t \gtrsim 10^3 \tau_\omega$. **Right:** Diffusion coefficient \mathcal{D}_{σ^*} as a function of σ^* obtained from DNS for $2 \times 10^3 \leq t/\tau_\omega \leq 10^4$ (\blacklozenge), and for the model (from Eq. (29)) for various values of α_{int} , as labelled.

algebraic, with a super-diffusive exponent that seems to depend on the shear rate. At much longer times, a diffusive behaviour is asymptotically reached. The time needed to reach the diffusive regime decreases with the shear rate. This behaviour can be explained in terms of the dependence upon σ^* of the velocity gradient Lagrangian correlation time (see inset of Fig. 3 right). Figure 7 (left) shows DNS measurements of the diffusion coefficient \mathcal{D}_{σ^*} as function of the shear rate σ^* . When σ^* increases, the diffusion coefficient becomes smaller because shear tends to deplete the structures of the flow. For the three largest values of shear, \mathcal{D}_{σ^*} becomes almost constant. This could originate from the fact that our simulations are performed in a finite-size domain. Indeed, when σ^* is large, the elongated structures of the flow start to get influenced by periodic boundary conditions and align with the direction of shear. This geometrical effect could affect our measurements.

The diffusion coefficient \mathcal{D}_{σ^*} obtained from Eq. (29) for the model is also shown in Fig. 7 (right) for different values of α_{int} . Its overall dependence upon σ^* is very similar to DNS data. However, one observes that the value $\alpha_{\text{int}} = 0.1$ of the fitting parameter that was previously used to reproduce the average angular displacement (Fig. 6 right) largely underestimates its variance. Quantitative agreements indeed require to choose $\alpha_{\text{int}} \approx 0.8$. The two statistics can thus not be reproduced with the same value of the fitting parameter. The needed increase of α_{int} to fit second-order statistics can be interpreted as a way for the stochastic model to compensate fat tails that develop in the distribution of angular increments, so that the contribution of large fluctuations is accounted for by a larger diffusion.

The violent fluctuations of angular increments are evidenced in Fig. 8, which shows the probability density function of $\delta\theta_t$ obtained from DNS at different times lags t and for $\sigma^* = 0$ (left panel) and $\sigma^* = 2.8$ (right panel). At first glance, one observes a strong qualitative difference between these two cases: Shear completely depletes fluctuations

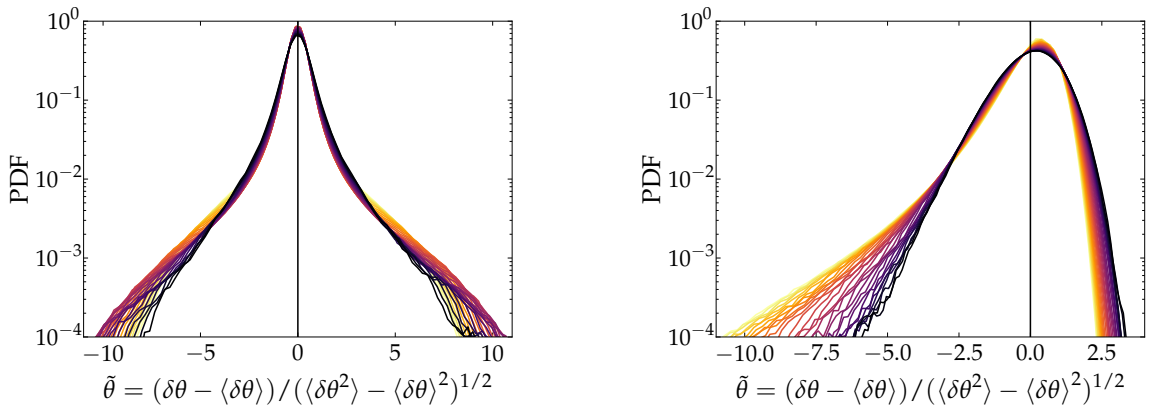


Figure 8: (Colour online) Probability density function (PDF) of the angular increment $\delta\theta_t = \theta_t - \theta_0$ centred and rescaled to unit variance for $\sigma^* = 0$ (left) and $\sigma^* = 2.6$ (right). The different curves correspond to various time lags logarithmically spaced between $t = 80 \tau_\omega$ and $t = 6000 \tau_\omega$ (from light yellow to dark violet).

at positive values, as already observed for vorticity (Fig. 1 right). Still the two cases share common features. First, as the time lag increases, the tails of both distributions tend to shrink and possibly approach a Gaussian behaviour. This is more evident for $\sigma^* > 0$ that shows an important depletion of large fluctuations when t increases. Second, one observes in both cases an intermediate asymptotic tail where the probability density decreases slower than an exponential. A log-log plot of the same data (not shown here) indeed reveals that $p(\delta\theta) \sim |\delta\theta|^{-\alpha}$ for increments of the order of 2 to 10 times their standard deviation and at moderate values of the time lag t . The exponent is independent of t but decreases as a function of the shear rate (it goes from $\alpha \approx 2.4$ when $\sigma^* = 0$ to $\alpha \approx 3.2$ when $\sigma^* = 2.6$). Such a behaviour is in line with the observations of Fig. 5 that show rods orientation experiencing intermittent (quasi-ballistic) excursions that we interpreted as a contribution of trapping by coherent vortical structures. Such a behaviour, together with its signature as a power law in the distribution of increments, strongly reminds what would be obtained if the rods angle were following a Lévy walk. Of course, jumps are bounded by the largest scales of the flow, ensuring that all moments of $\delta\theta_t$ converge. Still, this intermediate violent behaviour gives a large contribution at high orders, possibly explaining why the model cannot reproduce both the mean and the variance with the same amplitude factor α_{int} . Accounting for such effects would require to change paradigm and to model the orientation as a jump process rather than a pure diffusion.

V. CONCLUSIONS

To summarise, we have here studied the dynamics and statistics of rod-like particles transported by a homogeneous turbulent two-dimensional shear flow. We have introduced a Lagrangian stochastic model that is able to reproduce the combined effects of an average shear and of turbulent fluctuations on the orientation dynamics of such particles. The modelled velocity gradient is the superposition of a deterministic, stationary part and of random, delta-correlated-in-time component. This allowed us to derive analytical predictions for the statistics of the rods orientation, which were assessed by comparison to the results of direct numerical simulations.

We have first focused on single-time stationary statistics of the rods orientation. The model allowed us writing an explicit expression for the stationary probability density of the folded angle $\bar{\theta}$ in term of the solutions with a constant probability current of the associated Fokker–Planck equation. The dependence of this distribution upon the shear rate parameter σ^* is also explicit and eases comparison with DNS results. Three different expressions for the model fluid-gradient correlations were tested and our results reveals that orientation statistics are well reproduced only if both anisotropies and effects of long-time correlations of the Lagrangian velocity gradients are taken into account. Fine-tuning the model to fit DNS moreover requires to properly choose the value of a dimensionless parameter α_{int} , which controls the overall amplitude of velocity gradient fluctuations.

We then turned to two-time statistics and studied the evolution of the rods’ unfolded orientation over a given time lag. This led us to introduce two new definitions of the “tumbling rate”. The first, which solely applies in the presence of shear, is given by the asymptotic average angular velocity of the rods. It is directly proportional to the constant probability current of the stationary distribution and actually measures by how many turns per unit time the rods rotate under the influence of the mean shear. The second definition of a tumbling rate has the advantage to also apply in the absence of average shear. It is equal to the diffusion coefficient of the rods’ angular increment. These two tumbling rates can be derived analytically for the model. However, when comparing their values with DNS, one finds that they both require increasingly large values of the fitting fluctuation amplitude α_{int} . In short, our stochastic model is found to entail most important qualitative aspects of the orientation dynamics but reproducing quantitatively several high-order statistics cannot be done with a single value the fitting parameter.

We interpret such pitfalls as originating from rare, violent events in the orientation dynamics that occur when the rods are trapped in coherent vortical structures for extremely long times. Our model only accounts for the time-averaged contribution of such events, since it makes use of Lagrangian integral correlation times of fluid-velocity gradients. DNS results suggest that this might not be enough to reproduce the full distribution of angular increments. Nevertheless, to our view, this issue actually opens new modelling perspectives. The trajectories of the angular increment $\delta\theta_t$ are a combination of diffusion periods and long-range excursions, that strongly bring to mind known behaviours of Lévy walks. In this respect, further developments could consist in modelling the fluctuations of the fluid-velocity gradient in terms of an α -stable process, in an attempt to get a more realistic description of DNS. Such processes belong to the family of Lévy processes and are relatively straightforward to simulate. However, their use requires to introduce additional parameters that need to be calibrated, adding another level of complexity.

Finally let us stress that many aspects discussed in this article, and in particular the stochastic model that we introduce, straightforwardly extend to three-dimensional situations. The physics is however expected to be much richer, because different behaviours will arise depending whether the particles are rod or disk-shaped. We still expect to observe again non-trivial contributions from flow structures consisting of vortex tubes that tend to align with the span-wise direction [37]. We left three-dimensional extensions to future work.

ACKNOWLEDGMENTS

The authors are grateful to the OPAL infrastructure from Université Côte d'Azur for providing computational resources and support. We benefited from stimulating discussions with Christophe Henry and Dario Vincenzi who are warmly acknowledged. This work has been supported by the French government, through the UCA^{JEDI} Investments in the Future project managed by the National Research Agency (ANR) with the reference number ANR-15-IDEX-01, and by ANR through grant no. ANR-21-CE30-0040-01.

Appendix A: Itô's lemma on the orientation

We recall first the relation $\mathbf{B}_{ijnm}\mathbf{B}_{klmn} = 2\mathcal{D}_{ijkl}$, and introduce the notation:

$$\mathcal{D}_{ijkl} = \begin{pmatrix} \mathcal{D}_{1111} & \mathcal{D}_{1112} & \mathcal{D}_{1121} & \mathcal{D}_{1122} \\ \mathcal{D}_{1211} & \mathcal{D}_{1212} & \mathcal{D}_{1221} & \mathcal{D}_{1222} \\ \mathcal{D}_{2111} & \mathcal{D}_{2112} & \mathcal{D}_{2121} & \mathcal{D}_{2122} \\ \mathcal{D}_{2211} & \mathcal{D}_{2212} & \mathcal{D}_{2221} & \mathcal{D}_{2222} \end{pmatrix} = \begin{pmatrix} f & h & j & -f \\ & g & k & -h \\ \text{sym.} & & \ell & -j \\ & & & f \end{pmatrix}. \quad (\text{A1})$$

We derive the dynamics of the orientation angle $\bar{\theta} = \arctan(r_2/r_1)$, applying the Itô's Lemma to the separation vector in (10) ($d = 2$), that we rewrite first in its Itô form

$$dr_i = \langle A_{ij} \rangle r_j dt + \mathcal{D}_{jlij} r_l dt + \mathbf{B}_{ilk} r_l dw_t^k,$$

using the renumbering $\sum_{n,m=1}^2 \mathbf{B}_{ilnm} \partial W_{nm} = \sum_{k=1}^4 \mathbf{B}_{ilk} \partial w^k$, The multidimensional Ito's lemma applied to $\arctan(r_2/r_1)$ gives

$$d\bar{\theta} = \sum_{i,j} J_i^{\bar{\theta}} \langle A_{ij} \rangle r_j dt + \sum_{i,j,l} J_i^{\bar{\theta}} \mathcal{D}_{jlij} r_l dt + \frac{1}{2} \sum_{i,j,l,l'} \sum_k H_{ij}^{\bar{\theta}} (\mathbf{B}_{ilk} r_l \mathbf{B}_{j'l'k} r_{l'}) dt + \sum_{i,l} \sum_k J_i^{\bar{\theta}} \mathbf{B}_{ilk} r_l dw_t^k;$$

where $J_i^{\bar{\theta}} = -\sum_j^2 \varepsilon_{ij} r_j \|r\|^{-2}$ and $H_{ij}^{\bar{\theta}} = \sum_{l,l'}^2 (\varepsilon_{il} r_l r_j + \varepsilon_{j'l'} r_{l'} r_i) \|r\|^{-4}$ are respectively the gradient and Hessian matrix of $\arctan(r_2/r_1)$, denoting with ε_{ij} the 2D-Levi-Civita symbol, $\varepsilon_{ij} = \begin{pmatrix} 0 & 1 \\ -1 & 0 \end{pmatrix}$. In the equation above, the stochastic integral term can be reduced (with the help of the Brownian martingale representation – see e.g Karatzas and Shreve [51, Theorem 4.2, Chpt 3]) to a stochastic term (equivalent in law only) driven by a single Brownian motion (W_t), weighted with the diffusion matrix norm:

$$\begin{aligned} d\bar{\theta}^{\text{law}} &= \left(\sum_{i,j} J_i^{\bar{\theta}} \langle A_{ij} \rangle r_j dt + \sum_{i,j,l} J_i^{\bar{\theta}} \mathcal{D}_{jlij} r_l dt + \frac{1}{2} \sum_{i,j,l,l'} \sum_k H_{ij}^{\bar{\theta}} (\mathbf{B}_{ilk} r_l \mathbf{B}_{j'l'k} r_{l'}) \right) dt \\ &+ \left(\sum_k^4 \left(\sum_{i,l} J_i^{\bar{\theta}} \mathbf{B}_{ilk} r_l \right)^2 \right)^{\frac{1}{2}} dW_t \\ &= (\text{I} + \text{II} + \text{III}) dt + \text{IV} dW_t. \end{aligned} \quad (\text{A2})$$

We detail separately the computation of the four terms above.

Drift term I. Introducing $p_i = r_i/\|r\|$, i.e. $\mathbf{p} = (\cos \bar{\theta}, \sin \bar{\theta})$, and since the only component different from zero of $\langle A_{ij} \rangle$ is $\langle A_{12} \rangle = \sigma^*$,

$$\text{I} = \sum_{i,j} J_i^{\bar{\theta}} \langle A_{ij} \rangle r_j = - \sum_{i \neq m,j}^2 \varepsilon_{im} p_m \langle A_{ij} \rangle p_j = -\sigma^* p_2^2 dt = \frac{\sigma^*}{2} (\cos(2\bar{\theta}) - 1).$$

Drift term II. This contribution is identified to be zero: using again the definition of $J_i^{\bar{\theta}}$, and introducing the symmetries in matrix (A1)

$$\text{II} = - \sum_{i \neq \ell}^2 \varepsilon_{i\ell} p_\ell \sum_{j,l}^2 \mathcal{D}_{jlij} p_l = - \sum_{j,l}^2 (\mathcal{D}_{j1l1} p_2 p_l - \mathcal{D}_{j12j} p_1 p_l) = 0.$$

Drift term III. Developing the computation with the symmetries in matrix (A1):

$$\begin{aligned}
\text{III} &= \sum_{i,j,l,l'}^2 H_{ij}^{\bar{\theta}} \mathcal{D}_{iljl'} r_l r_{l'} = \sum_{i \neq m}^2 \sum_{j \neq n}^2 \sum_{l,l'}^2 \mathcal{D}_{iljl'} (\varepsilon_{im} p_m p_j + \varepsilon_{jn} p_n p_i) p_l p_{l'} \\
&= 2 \sum_{l,l'}^2 \left((\mathcal{D}_{111l'} - \mathcal{D}_{212l'}) p_1 p_2 + \frac{1}{2} (\mathcal{D}_{112l'} + \mathcal{D}_{211l'}) (p_2^2 - p_1^2) \right) p_l p_{l'} \\
&= 2 \left(3(j+h) p_1^2 p_2^2 - j p_1^4 - h p_2^4 + (2f - \ell - k) p_1^3 p_2 + (-2f + g + k) p_2^3 p_1 \right).
\end{aligned}$$

Next, introducing the following equalities from Cartesian to polar coordinates

$$\begin{aligned}
p_1^3 p_2 &= \frac{1}{4} (\sin(2\bar{\theta}) + \frac{1}{2} \sin(4\bar{\theta})), & p_1^2 p_2^2 &= \frac{1}{8} (1 - \cos(4\bar{\theta})), & p_1^4 &= \frac{1}{8} (3 + 4 \cos(2\bar{\theta}) + \cos(4\bar{\theta})), \\
p_2^3 p_1 &= \frac{1}{4} (\sin(2\bar{\theta}) - \frac{1}{2} \sin(4\bar{\theta})), & & & p_2^4 &= \frac{1}{8} (3 - 4 \cos(2\bar{\theta}) + \cos(4\bar{\theta})),
\end{aligned}$$

$$\text{III} = -\frac{\gamma_3}{2} \sin(2\bar{\theta}) - \gamma_4 \sin(4\bar{\theta}) + \frac{\gamma_1}{2} \cos(2\bar{\theta}) + \gamma_2 \cos(4\bar{\theta}),$$

with

$$\begin{aligned}
\gamma_1 &= 2(h-j) & \gamma_2 &= -h-j \\
\gamma_3 &= \ell - g & \gamma_4 &= -f + \frac{1}{2}k + \frac{1}{4}(\ell + g).
\end{aligned} \tag{A3}$$

Diffusion term IV. We denoted this coefficient $b(\mathbf{p})$, with $b^2(\mathbf{p}) = \sum_k^4 \left(\sum_{i,l} J_i^{\bar{\theta}} \mathbf{B}_{ilk} r_l \right)^2$. Using $(J_1^{\bar{\theta}} r_l, J_2^{\bar{\theta}} r_l) = (-p_2 p_l, p_1 p_l)$

$$b^2(\mathbf{p}) = \sum_k^4 \left(-p_2 p_1 \mathbf{B}_{11k} + p_1^2 \mathbf{B}_{21k} - p_2^2 \mathbf{B}_{12k} + p_1 p_2 \mathbf{B}_{22k} \right)^2.$$

Denoting \mathbf{B}_{ijk} as the 4×4 matrix $\mathbb{B} = B_{2(i-1)+j,k}$, and $v(p)$ the \mathbb{R}^4 element $(-p_1 p_2, -p_2^2, p_1^2, p_1 p_2)$, we obtain

$$b^2(\mathbf{p}) = \|\mathbb{B}v(\mathbf{p})\|^2 = v(\mathbf{p})^t \mathbb{B}^t \mathbb{B} v(\mathbf{p}) = 2v(\mathbf{p})^t \mathbb{D} v(\mathbf{p}) = 2\{(4f - 2k)p_1^2 p_2^2 + 4hp_2^3 p_1 - 4jp_1^3 p_2 + \ell p_1^4 + gp_2^4\}. \tag{A4}$$

Using next the polar coordinates relations introduced earlier

$$b^2(\bar{\theta}) = \gamma_0 + \gamma_1 \sin(2\bar{\theta}) + \gamma_2 \sin(4\bar{\theta}) + \gamma_3 \cos(2\bar{\theta}) + \gamma_4 \cos(4\bar{\theta}),$$

where $\gamma_0 = f + \frac{1}{2}k + \frac{3}{4}(\ell + g)$. We report in Table I, the measured values of γ_i , for $\mathcal{D}^{\text{aniso}}(\sigma^*)$ and $\mathcal{D}^{\text{int}}(\sigma^*)$.

Appendix B: Strict positivity of the folded angle diffusion coefficient b

The strict positivity of b is required to develop analytical expressions through the stochastic approach. We discuss here the three cases studied in this paper. To facilitate the discussion, we start from the expression (A4) for b^2 expressed with the Cartesian coordinates.

a. The \mathcal{D}^{iso} case simplifies (A4) with $f = -k =, g = l = 3f, h = j = 0$, and so

$$b^2(\mathbf{p}) = 6fp_1^2 p_2^2 + 3fp_1^4 + 3fp_2^4 = 3f > 0.$$

b. The $\mathcal{D}^{\text{aniso}}$ case (see Fig. 3 (left)) allows to minorate (A4) with $0 \leq f = -k, 0 \leq f \leq l \leq g, 0 \leq j \leq f$ and $k \leq h \leq 0$. Assuming first $|p_1| \leq |p_2|$, then $4hp_2^3 p_1 > 4hp_2^4, -4jp_1^3 p_2 > -4jp_1^2 p_2^2$, and

$$\begin{aligned}
b^2(\mathbf{p}) &= 6fp_1^2 p_2^2 + 4hp_2^3 p_1 - 4jp_1^3 p_2 + gp_2^4 + lp_1^4 \geq 6fp_1^2 p_2^2 + 4hp_2^4 - 4jp_1^2 p_2^2 + gp_2^4 + lp_1^4 \\
&= (6f - 4j)p_1^2 p_2^2 + (g + 4h)p_2^4 + lp_1^4 \geq \min\{(6f - 4j)/2, (g + 4h), l\}.
\end{aligned}$$

Assuming next $|p_1| \geq |p_2|$, we also consider that $(l + 4h) > 0$ in Fig. 3 (left). Then

$$\begin{aligned}
b^2(\mathbf{p}) &= 6fp_1^2 p_2^2 + 4hp_2^3 p_1 - 4jp_1^3 p_2 + gp_2^4 + lp_1^4 \geq 6fp_1^2 p_2^2 + 4hp_2^2 p_1^2 - 4jp_1^4 + gp_2^4 + lp_1^4 \\
&= (6f + 4h)p_1^2 p_2^2 + (l - 4j)p_1^4 + gp_2^4 \geq \min\{(6f + 4h)/2, (l - 4j), g\}.
\end{aligned}$$

So for any p ,

$$b^2(\mathbf{p}) \geq \min\{(6f - 4j)/2, (g + 4h), l\} \wedge \min\{(6f + 4h)/2, (l - 4j), g\}.$$

According to Figure 3 (left), the smallest term above is $(l - 4j) > 0$. The diffusion is then strictly positive for the considered values of shear.

σ^*	0.00	0.03	0.07	0.15	0.33	0.77	1.26	1.77	2.80	3.79	
γ_0	$\mathcal{D}^{\text{aniso}}$	0.7565	0.7559	0.7612	0.7433	0.7311	0.7084	0.7210	0.7223	0.7065	0.7389
	\mathcal{D}^{int}	66.8319	49.3522	36.7193	21.4299	12.3579	7.7984	6.5343	6.0211	6.0748	8.0637
γ_1	$\mathcal{D}^{\text{aniso}}$	0.0033	-0.0008	-0.0160	-0.0734	-0.1642	-0.1883	-0.1665	-0.1518	-0.1165	-0.1007
	\mathcal{D}^{int}	0.6818	0.2007	0.2778	-0.6735	-2.4257	-1.3606	-0.7794	-0.6748	-0.4338	-0.3979
γ_2	$\mathcal{D}^{\text{aniso}}$	-0.0015	-0.0002	-0.0022	-0.0027	0.0052	0.0317	0.0442	0.0455	0.0394	0.0354
	\mathcal{D}^{int}	0.0034	0.0184	-0.0002	-0.0171	0.0581	0.2195	0.1815	0.1779	0.1428	0.149452
γ_3	$\mathcal{D}^{\text{aniso}}$	-0.0095	-0.0014	-0.0032	-0.0179	-0.1031	-0.2961	-0.4134	-0.4818	-0.5741	-0.7004
	\mathcal{D}^{int}	-0.1937	0.0441	-0.2509	-0.5446	-2.1580	-3.6875	-4.4623	-4.9191	-5.9903	-9.2379
γ_4	$\mathcal{D}^{\text{aniso}}$	0.0028	0.0021	0.0004	-0.0004	-0.0057	0.0043	0.0328	0.0528	0.0885	0.1300
	\mathcal{D}^{int}	0.0477	0.0058	0.0460	0.0235	-0.0264	0.2027	0.4348	0.5986	0.9369	1.7944

Table I: Values of γ_i (with $i = 0, \dots, 4$) used in the model (in the normalised case, *i.e.* by multiplying for τ_ω) when we use $\mathcal{D}^{\text{aniso}}$ or \mathcal{D}^{int} to study the model as a function of the shear rate σ^* . Here, the values of the tuning parameters are $\alpha_{\text{aniso}} = \alpha_{\text{int}} = 1$.

c. The \mathcal{D}^{int} case (see Fig. 3 (right)) simplifies (A4) with $f = h = j = 0$, $k \leq 0$, $g > l > 0$ to

$$b^2(p) = -2kp_1^2p_2^2 + gp_2^4 + lp_1^4 = l - 2(l+k)p_1^2p_2^2 + (g-l)p_2^4 > 0.$$

The diffusion is then again strictly positive for the considered values of shear.

-
- [1] F. Lundell, L. D. Söderberg, and P. H. Alfredsson, *Annu. Rev. Fluid Mech.* **43**, 195 (2011).
[2] R. C. Moffet and K. A. Prather, *Proc. Natl. Acad. Sci. U.S.A.* **106**, 11872 (2009).
[3] L. Sabban, A. Cohen, and R. van Hout, *J. Fluid Mech.* **814**, 42 (2017).
[4] M. M. Musielak, L. Karp-Boss, P. A. Jumars, and L. J. Fauci, *J. Fluid. Mech.* **638**, 401 (2009).
[5] K. Vercruyse, R. C. Grabowski, and R. Rickson, *Earth Sci. Rev.* **166**, 38 (2017).
[6] J. E. Butler and B. Snook, *Annu. Rev. Fluid Mech.* **50**, 299 (2018).
[7] M. Daghooghi and I. Borazjani, *J. Fluid Mech.* **781**, 506 (2015).
[8] G. B. Jeffery, *Proc. Roy. Soc. Lond. A* **102**, 161 (1922).
[9] S. Parsa, J. S. Guasto, M. Kishore, N. T. Ouellette, J. Gollub, and G. A. Voth, *Phys. Fluids* **23**, 043302 (2011).
[10] G. Bellani, M. L. Byron, A. G. Collignon, C. R. Meyer, and E. A. Variano, *J. Fluid Mech.* **712**, 41 (2012).
[11] S. Parsa and G. A. Voth, *Phys. Rev. Lett.* **112**, 024501 (2014).
[12] G. G. Marcus, S. Parsa, S. Kramel, R. Ni, and G. A. Voth, *New J. Phys.* **16**, 102001 (2014).
[13] S. Bounoua, G. Bouchet, and G. Verhille, *Phys. Rev. Lett.* **121**, 124502 (2018).
[14] A. Pumir and M. Wilkinson, *New J. Phys.* **13**, 093030 (2011).
[15] S. Parsa, E. Calzavarini, F. Toschi, and G. A. Voth, *Phys. Rev. Lett.* **109**, 134501 (2012).
[16] P. Mortensen, H. Andersson, J. Gillissen, and B. Boersma, *Phys. Fluids* **20**, 093302 (2008).
[17] E. Calzavarini, L. Jiang, and C. Sun, *Phys. Fluids* **32**, 023305 (2020).
[18] M. Wilkinson, V. Bezuglyy, and B. Mehlig, *Phys. Fluids* **21**, 043304 (2009).
[19] M. Shin and D. L. Koch, *J. Fluid Mech.* **540**, 143 (2005).
[20] G. A. Voth and A. Soldati, *Annu. Rev. Fluid Mech.* **49**, 249 (2017).
[21] B. K. Brunk, D. L. Koch, and L. W. Lion, *J. Fluid Mech.* **364**, 81 (1998).
[22] D. Vincenzi, *J. Fluid Mech.* **719**, 465 (2013).
[23] S. Girimaji and S. Pope, *Phys. Fluids A* **2**, 242 (1990).
[24] M. Chertkov, A. Pumir, and B. I. Shraiman, *Phys. Fluids* **11**, 2394 (1999).
[25] L. Chevillard and C. Meneveau, *Phys. Rev. Lett.* **97**, 174501 (2006).
[26] L. Biferale, L. Chevillard, C. Meneveau, and F. Toschi, *Phys. Rev. Lett.* **98**, 214501 (2007).
[27] L. Chevillard and C. Meneveau, *J. Fluid Mech.* **737**, 571 (2013).
[28] R. M. Pereira, L. Moriconi, and L. Chevillard, *J. Fluid Mech.* **839**, 430 (2018).
[29] A. Celani, A. Puliafito, and K. Turitsyn, *EPL* **70**, 464 (2005).
[30] K. Turitsyn, *J. Exp. Theor. Phys.* **105**, 655 (2007).
[31] E. L. C. V. M. Plan and D. Vincenzi, *Proc. Roy. Soc. Lond. A* **472**, 20160226 (2016).
[32] C. Henry, G. Krstulovic, and J. Bec, *Phys. Rev. E* **98**, 023107 (2018).
[33] G. K. Batchelor, *J. Fluid Mech.* **5**, 113 (1959).

- [34] R. Kraichnan, *Phys. Fluids* **11**, 945 (1968).
- [35] G. Falkovich, K. Gawędzki, and M. Vergassola, *Rev. Mod. Phys.* **73**, 913 (2001).
- [36] R. Rogallo, *Numerical experiments in homogeneous turbulence*, Tech. Rep. TM-81315 (NASA Ames Research Center, California, 1981).
- [37] A. Pumir, *Phys. Fluids* **8**, 3112 (1996).
- [38] E. Lindborg and K. Alvelius, *Phys. Fluids* **12**, 945 (2000).
- [39] N. E. L. Haugen and A. Brandenburg, *Phys. Rev. E* **70**, 026405 (2004).
- [40] U. Frisch, S. Kurien, R. Pandit, W. Pauls, S. S. Ray, A. Wirth, and J.-Z. Zhu, *Phys. Rev. Lett.* **101**, 144501 (2008).
- [41] G. Boffetta and R. E. Ecke, *Annu. Rev. Fluid Mech.* **44**, 427 (2012).
- [42] G. Falkovich and V. Lebedev, *Phys. Rev. E* **83**, 045301 (2011).
- [43] R. Ni, N. T. Ouellette, and G. A. Voth, *J. Fluid Mech.* **743**, R3 (2014).
- [44] R. T. Pierrehumbert and H. Yang, *J. Atmos. Sci.* **50**, 2462 (1993).
- [45] E. Balkovsky and A. Fouxon, *Phys. Rev. E* **60**, 4164 (1999).
- [46] M. S. Borgas, B. L. Sawford, S. Xu, D. A. Donzis, and P.-K. Yeung, *Phys. Fluids* **16**, 3888 (2004).
- [47] T. Peacock and G. Haller, *Physics Today* **66**, 41 (2013).
- [48] F. Castell, *Probab. Theory Relat. Fields* **96**, 225 (1993).
- [49] E. García-Portugués, M. Sørensen, K. V. Mardia, and T. Hamelryck, *Stat. Comput.* **29**, 1 (2019).
- [50] J. C. Mattingly, A. M. Stuart, and M. V. Tretyakov, *SIAM J. Numer. Anal.* **48**, 552 (2010).
- [51] I. Karatzas and S. Shreve, *Brownian motion and stochastic calculus*, Vol. 113 (Springer Science & Business Media, 2012).